Chapter

Modeling of Olivine and Clinopyroxene Fractionation in Intracontinental Alkaline Basalts: A Case Study from the Carpathian-Pannonian Region

Tamás Sági, Szabolcs Harangi and Theodoros Ntaflos

Abstract

Besides mantle peridotites primary basaltic melts are the best tool to investigate upper mantle petrology and geochemistry. However, de facto primitive melts are hard to found, as basaltic melts usually go through a fractionation process during their ascent towards the surface. Most primary melt calculators are based on the major or trace element compositions of olivine-phyric ocean island basalts and peridotites and are less accurate if clinopyroxene fractionation occurred. In this chapter a new fractionation modeling method of alkaline basalts will be introduced, which has been published earlier only in Hungarian. Olivine $\pm$ clinopyroxene fractionation of four basaltic volcanoes have been modeled from different Miocene-Quaternary volcanic fields from the Carpathian-Pannonian Region (Stiavnica (Selmec) VF, Novohrad-Gemer (Nógrád-Gömör) VF, Perşani Mts. (Persányi Mts.) VF and from the Lucaret-Sanoviţa (Lukácskő-Sziklás) volcano.

Keywords: olivine, clinopyroxene, fractionation, intracontinental, monogenetic, alkaline basalt

1. Introduction

Intracontinental monogenetic alkaline basaltic volcanic fields consist of various types of small-scale volcanoes (e.g. scoria cones, tuff rings, maars, diatremes and related lava flows) [1]. However, the size of the volcanic edifices is usually smaller than 1 km^3 and they are short-lived volcanoes, the total magma output rate of a monogenetic volcanic field can be compared with a polygenetic volcano [1]. The lifespan of the volcanic field can last for several millions of years (e.g. [2, 3]). Based on the geochemical and petrographic characteristics of the individual volcanoes, monogenetic basaltic volcanic fields could be very diverse both spatially and temporally (e.g. [4]). This diversity depends on several factors. Basaltic melt could be generated in the asthenosphere or in the lithosphere. Partial melting of the asthenosphere could be caused by a mantle plume (e.g. [5–7]), or mantle flows related to active rifting, collision or lithospheric delamination (e.g. [8–10]). Melt generation in the lithospheric mantle is often related to metasomatized peridotites

and pyroxenites which are rich in volatiles and alkalis (e.g. [3, 11–13]). Primitive alkaline basalts are excellent tools to study the petrological and geochemical heterogeneity and thermal characteristics of the upper mantle and the type of melt generation (e.g. [5, 14–17]), however a seemingly primitive basaltic magma could have undergone fractionation [18]. Only with fairly accurate knowledge on the primary melt composition it is possible to reveal the whole story and characterize the source region of the basalts (e.g. [14, 19, 20]).

To find primary melt compositions we have to study their ascent history and characterize the melt evolution from the source to the surface. Most common methods are based on the main and trace elements composition of the bulk rock (e.g. [14, 18–21]), and these methods are often less accurate if clinopyroxene fractionation occurred or if the source rock contained pyroxenite. To avoid the "pyroxene problem" a new olivine +/− clinopyroxene fractionation method has been developed by [22] and first published by [23] in Hungarian. Here we will show the method accuracy and some fractionation calculation results of alkaline basalts from [22, 23].

2. Concept of olivine and clinopyroxene fractionation modeling

Primitve magma compositions derived from less fractionated alkaline basalts are key tools to characterize the source region of upper mantle melts (i.e. petrology and geochemistry, depth and degree of melting, potential temperature of the upper mantle) (e.g. [7, 14, 17, 19, 24, 25]).

Most well-known primitive melt calculations are based on olivine addition or subtraction from bulk rock compositions of alkaline basalts from OIBs and LIPs [14, 19, 20, 24]. These methods could be misleading if the source rock of the basalt wasn't purely peridotitic and especially if not only olivine but clinopyroxene fractionation occurred [14]. Olivine addition to rocks that were generated from eclogitic/pyroxenitic mantle or went through clinopyroxene fractionation can produce unrealistically primitive melt compositions with too high MgO content, Mg# and mantle potential temperature [14].

Even primitive, high Mg# intracontinental alkaline basaltic rocks could be derivative melts after olivine and deep-seated clinopyroxene fractionation [18]. To develop a more realistic fractionation modeling method instead of pure olivine addition/subtraction the degree of clinopyroxene fractionation should be taken into account. During fractional crystallization both melt and newly-formed crystals' composition will change continuously. If this process can be modeled, an estimate for the degree of crystallization and for the main elements composition of the parental melt can be given.

To find the degree of olivine ± clinopyroxene fractionation quantitative estimations were performed.

With increasing degree of fractional crystallization of an alkaline basaltic melt the Fo and Ni content of olivine crystals will decrease. As it is a minor/trace element, the concentration of Ni in olivine depends on the D_{Ni}^{ol-liq}. In accordance with results of [26] it was suggested by [27] that on the Fo-Ni plot of olivines from an alkaline basalt the olivine-only fractionation would appear as a curve of exponentially decreasing Ni-content with decreasing Fo-content, while co-crystallization of olivine and clinopyroxene draws a linear (diagonal or nearly horizontal) trend on the same plot. The slope of the exponential curve is determined by the D_{Ni}^{ol-liq}, while the slope of the linear section depends on the $D_{Ni}^{(ol+cpx)-liq}$. It has been shown on olivine and clinopyroxene phyric rock samples that the primitive

(Fo and Ni-rich) population of olivine crystals will cluster dominantly around the upper part of the predicted exponential curve on the Fo-Ni plot and with decreasing Ni and Fo content at some point – when the clinopyroxene also begins to crystallize - the curve will change to diagonal [27]. Accordingly if other significant process that can modify the Fo-Ni pattern of olivines than crystallization of olivine and clinopyroxene can be ruled out, the degree of fractional crystallization of the two mineral phases can be estimated based on the composition of the olivine crystals and the bulk rock. The Fo-Ni pattern of fresh, unaltered olivine crystals depends on the Mg# and/or the Ni-content of the basaltic melt. Significant change in Mg# of alkaline basaltic melts – besides olivine ± clinopyroxene fractionation – could be caused by fractionation of amphibole or by incorporation of Mg/Fe rich minerals (olivine, clinopyroxene, amphibole and magnetite). The Ni-content of olivines during fractional crystallization could be changed by precipitation of minerals with $D_{Ni}^{min-liq}$ higher than 1. This value is the highest for magnetite (up to 30) and olivine (up to 25), and almost a magnitude lower for clinopyroxene (1–3) and amphibole (0.6–3) [28–31]. To avoid any processes than olivine and clinopyroxene fractionation during magma ascent the following filters have been used during sample selection. 1: only fresh, unaltered olivine and olivine-clinopyroxene phyric basalts without amphibole content were investigated. 2: samples contain only minor magnetite content (<1%) with very low Ni concentration (200–700 ppm). 3: there is no sign of olivine or clinopyroxene incorporation (mega- or antecrysts with significantly different petrographic or geochemical characteristics.

2.1 The steps of the modeling

1. Creating a corrected major elements composition for each rock sample from LOI-free raw data: redistributing the $Fe_2O_3^{tot}$ content into FeO and Fe_2O_3 assuming a Fe^{3+}/Fe^{2+} ratio of 0.15; recalculating Ni and Cr concentrations from ppm into NiO and Cr_2O_3 wt. % values. The Fe^{3+}/Fe^{2+} will be reflected in the *Mg#* of the rock ($Mg\#_{rock} = Mg/(Mg + Fe^{2+}) \times 100$, where Mg and Fe^{2+} are cation fractions. A different Fe^{3+}/Fe^{2+} ratio (and Mg#) of the rock would modify later calculations (e.g. the amount of olivine that is calculated in the 2nd step) as they will lead to another equilibrium olivine composition. Therefore highly oxidized samples cannot be used as they have significantly higher Fe^{3+} content and lower $Mg\#_{rock}$. If the exact ratio of Fe^{3+}/Fe^{2+} is known, it must be used instead of 0.15.

2. Calculating the Fo content of a hypothetical olivine (Fo*) being in equilibrium with the bulk rock composition, using the equation of Fo (mol%) = 100-(X/(1 + X)*100), where X = ([100*$K_{D_{Fe-Mg}}^{ol-liq}$]-[$Mg\#_{rock}$])/ $Mg\#_{rock}$ and $K_{D_{Fe-Mg}}^{ol-liq}$ = 0.3. If the difference between the calculated equilibrium Fo value (= Fo*) and the Fo content of the most primitive (richest in Ni and probably in Fo) olivine ($Fo_{ol^{Ni\_max}}$) exceeds 0.1 mol%: the bulk rock composition has to be modified by olivine addition or subtraction in portions of 0.1 wt. % to reach equilibrium as follows (**Figure 1A**).

   a. If Fo* < $Fo_{ol^{Ni\_max}}$: the composition of an olivine crystal (being in equilibrium with the instantaneous melt) has to be added to the bulk rock composition in steps of 0.1 wt. %. For this, real analyzed olivine compositions from the same rock can be used.

   b. If Fo* > $Fo_{ol^{Ni\_max}}$: the composition of the most primitive olivine (ol^{Ni_max}) has to be subtracted from the bulk rock composition in steps of 0.1 wt. %.
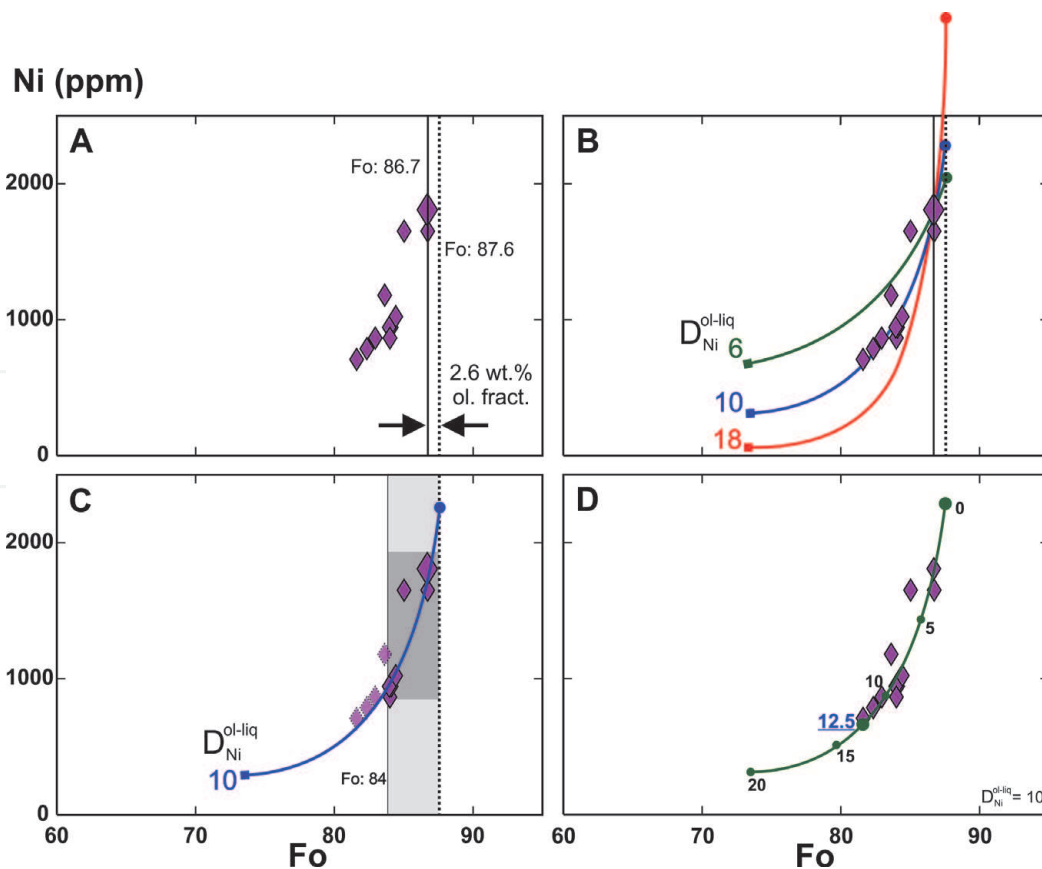
Figure 1.
An example of olivine fractionation modeling (BRE basanite olivine Fo-Ni plots). A) the most primitive olivine phenocryst is not in equilibrium with the bulk rock composition. The difference between the most Ni-rich olivine (large symbol, $Fo_{86.7}$) and a hypothetical olivine being in equilibrium with the bulk rock ($Fo_{87.6}$) can be explained by 2.6 wt. % olivine fractionation. B) Calculation of olivine fractionation curves with different values of D_{Ni}^{ol-liq}. Starting point for calculation is the most Ni-rich olivine (large symbol, 1807 ppm Ni, $Fo_{86.7}$), from where the fractionation curve should be modeled by olivine addition (until reaching equilibrium with the bulk rock at $Fo_{87.6}$ olivine) and by olivine subtraction (until reaching 20 wt. % olivine fractionation, lower end of the curves). The Ni-content of the hypothetical, most primitive olivine ($Fo_{87.6}$) varies between 2061 and 2828 ppm, depending on the applied D_{Ni}^{ol-liq} value. C) Based on the composition of the most primitive olivine phenocrysts (olivine population over the 75th percentile by Fo-content or over Fo_{84}; marked by gray background) the best fitting olivine fractionation curve should be selected to assign the D_{Ni}^{ol-liq} of the rock. In this example the olivine fractionation curve related to $D_{Ni}^{ol-liq} = 10$ was selected. D) As the total olivine phenocryst population fits well to the selected fractionation curve, only olivine fractionation can be assumed. Green dots and numbers (wt. %) along the curve represent increasing olivine fractionation. The degree of olivine fractionation is 12.5 wt. %, it is marked by the most evolved crystal ($Fo_{81.6}$, Ni = 707 ppm). For a detailed description of fractionation modeling see the appendix of [23].

The amount of subtracted or added olivine (in wt. %) could represent the difference between the melt composition represented by the bulk rock and by the equilibrium melt related to the most primitive olivine in the sample. We call this 'initial olivine fractionation'.

3. Calculating hypothetical (pure) olivine fractionation curves for $D_{Ni}^{ol-liq} = 5 - 20$ [29] on the Fo-Ni plot. The higher the D_{Ni}^{ol-liq}, the smoother the fractionation curve (**Figure 1B**).

   a. Modeling the decrease of MgO and Fo content in the melt and in equilibrium olivines simultaneously due to fractionation. Starting melts composition (Step 1.) has to be in equilibrium with the most Ni-rich olivine. Fractionation can be modeled by subtracting olivine in portions of 0.1 wt. % from the melt until 20 wt. % of total fractionation. During

calculation composition of analyzed olivine crystals (being nearly in equilibrium with the instantaneous melt) should be applied.

b. Whereas the decrease of Fo content in olivines during fractionation has been calculated with a constant $K_{D_{Fe-Mg}}^{ol-liq}$ (0.3), the decrease of Ni concentration in the fractionated olivine crystals and in the equilibrium melt have to be modeled for each D_{Ni}^{ol-liq} value between 5 and 20, assuming Rayleigh fractionation. Ni content of the most Ni-rich, analyzed olivine crystal is taken as starting data.

4. Determination of the D_{Ni}^{ol-liq} of the investigated basalts.

   Based on [27] in the case of pure olivine fractionation the most primitive olivine crystals should cluster along the upper, steep part of an exponential curve on the Fo-Ni plot. The most Mg-rich analyzed olivine crystals (over the 75th percentile by Fo-content and or over Fo_{84}) are compared to the calculated Fo-Ni curves (Step 2.) with the least squares method, and the best-fitting one will be accepted for the D_{Ni}^{ol-liq} of the investigated basalt (**Figure 1C**).

5. Estimation of the degree of the pure olivine fractionation.

   The hypothetical, pure olivine fractionation trajectory should be compared with the total olivine Fo-Ni dataset of the sample, whether they are fitting well, or at some point the initially exponential trend of analyzed olivine crystals changes to a more straight, diagonal one.

   a. If they are fitting well, only olivine fractionation happened. The olivine crystal with lowest Fo-Ni content will draw the degree of fractionation, which can be easily read from the modeled Fo-Ni curve (**Figure 1D**). In this case the modeling has been ended here. Jump to Step 7.

   b. If the trend of the analyzed olivine crystals can be divided into an exponential and a linear section, the first part represents the initial pure olivine fractionation and the linear part the later olivine-clinopyroxene co-crystallization. The degree of pure olivine fractionation is determined by the intersection of the modeled olivine Fo-Ni curve and the linear section of the olivine dataset (**Figure 2**).

6. Modeling of the olivine+clinopyroxene co-crystallization (**Figure 2B**). The applied value of D_{Ni}^{ol-liq} has been selected in Step 3, while for $D_{Ni}^{cpx-liq}$ a constant value of 2.8 should be used [31].

   a. Calculating the composition of the equilibrium melt ('intermediate melt') for the olivine that represents the end of the initial pure olivine fractionation (Step 4a.) like equilibrium melt calculations in Step 1.

   b. Modeling the evolution of the "intermediate melt" by fractionation of olivine and clinopyroxene together. The decrease of olivines Ni concentration along the diagonal Fo-Ni trend has to be modeled by Rayleigh fractionation presuming different olivine/clinopyroxene ratios. As a thought experiment, the decrease of Ni concentration in olivines could be modeled by a given quantity of olivine (X wt. %) or
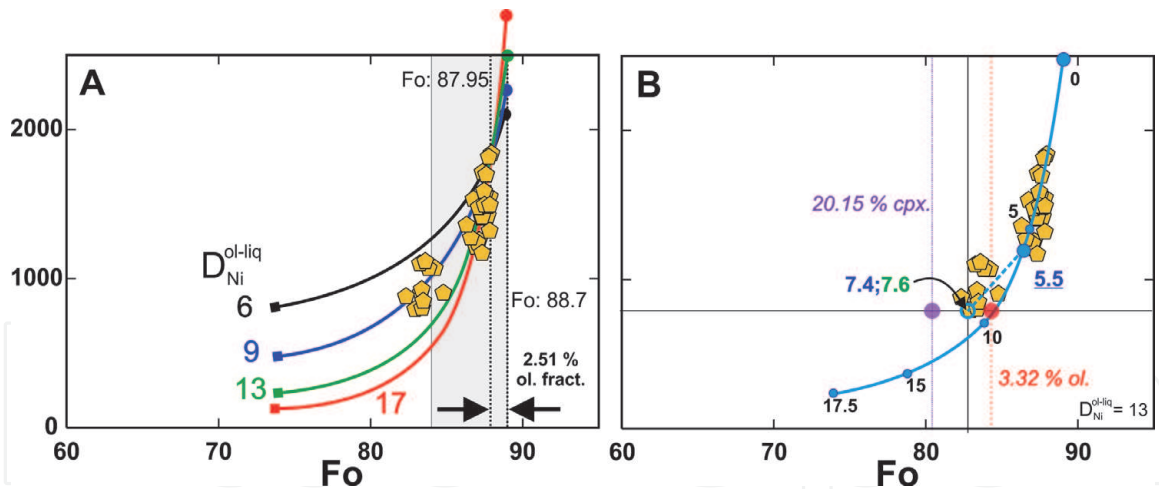
Figure 2.
*An example of olivine and clinopyroxene fractionation modeling (SOR basanite olivine Fo-Ni plots). A) the most primitive olivine phenocryst ($Fo_{87.95}$) is not in equilibrium with the bulk rock composition. Olivine fractionation curves were modeled as in **Figure 1**. The most primitive olivine phenocrysts (marked by gray background) suggest a D_{Ni}^{ol-liq} value of 13, however the geochemical diversity of the total olivine population cannot be explained by pure olivine fractionation, as olivine crystals ($<Fo_{83.6}$) do not fit the curve. B) Based on the modeled Fo-Ni curve of $D_{Ni}^{ol-liq}=13$ an initial olivine fractionation of 5.5 wt. % can be assumed. The composition of the more evolved olivine crystals ($< Fo_{83.6}$) suggest that besides olivine the fractionation of clinopyroxene has also begun [27]. The co-crystallization of the two minerals (i.e. the effect of clinopyroxene crystallization on olivine composition) can be modeled by the olivine population between the least primitive olivine crystal that fits to the calculated fractionation curve ($Fo_{86.3}$, Ni = 1186 ppm) and the most evolved crystal ($Fo_{83.4}$, Ni = 801 ppm). The decrease of Ni concentration (400 ppm) and Fo content (2.9 Mol%) in this olivine population have to be explained. If only olivine or clinopyroxene crystallization had occurred, the 400 ppm drop in Ni-concentration could be explained by 3.32 wt. % olivine or by 20.15 wt. % clinopyroxene fractionation (with a $D_{Ni}^{ol-liq}=13$ and $D_{Ni}^{cpx-liq}=2.8$ [31]). If this had happened, at the end of the fractionation, the Fo concentration of olivine crystals would have been $Fo_{84.3}$ (red dashed line and circle) or $Fo_{80.4}$ (purple dashed line and circle), respectively. None of them match the composition of the most evolved olivine crystal ($Fo_{83.4}$), therefore a co-crystallization of olivine and clinopyroxene must be assumed. The fractionation of the basaltic melt being in equilibrium with the $Fo_{86.3}$ olivine has been modeled with several different olivine/clinopyroxene ratio and amount. Fractionation of 2 wt. % olivine and 8 wt. % clinopyroxene would create a basaltic melt that would be in equilibrium with the most evolved analyzed olivine crystal ($Fo_{83.4}$). Because fractionation of 5.5 wt. % olivine had already taken place before this, the total degree of fractionation would be 7.39 wt. % olivine and 8.56 wt. % clinopyroxene (Initial olivine fractionation: 5.5 wt. %. Olivine and clinopyroxene co-crystallization: 0.945 × 2 = 1.89 wt.% olivine and 0.945 × 8 = 7.56 wt.% clinopyroxene. Altogether 7.39 wt. % olivine and 7.56 wt. % clinopyroxene fractionation.). For a detailed description of fractionation modeling see the appendix of [23].*

clinopyroxene (Y wt. %) fractionation only, however it must be a co-crystallization of the two minerals. Therefore, the decrease of Ni by fractional crystallization has to be calculated for each ol/cpx ratio from X wt. % olivine +0 wt. % clinopyroxene to 0 wt. % olivine + Y wt. % olivine, changing the amount of each mineral by steps of 0.1 wt. %.

c. Estimating the compositional change of the intermediate melt for all ratios of ol/cpx by subtracting these minerals from it. Subtraction of minerals is the same as in Step 1a. The calculated melt compositions are considered "final melts".

d. Estimating the Fo-content of equilibrium olivine for each final melt composition and compare them to the analyzed olivine crystals.

e. That olivine/clinopyroxene fractionation ratio and amount will be accepted, for which the related final melts equilibrium olivine will have the same Fo-content as the lower end of the diagonal Fo-Ni trend of analyzed olivines.

7. The total degree of olivine and clinopyroxene fractionation will be the sum of the volumes calculated in "Step 4b" and "Step 5e".

8. To find the major element composition of the parental melt (**Table 3**) the summerized amount of olivine or olivine+clinopyroxene have to be added to the bulk rock composition (**Tables 1** and **2**).

9. Optional check: it is possible to calculate parental melt composition by another method based only on olivine addition, like the method of PRIMELT2 [14] or Fractionate-PT [19]. If significant amount (>10 wt. %) fractionation of clinopyroxene has been calculated by the presented method, the mentioned programs should calculate a more Mg-rich parental melt (**Figure 3** and **Table 3**).

2.2 Remarks on limitations of the presented fractionation estimation method

1. Alkaline basalts that are derivative melts of fertile mantle peridotites will have an MgO content of 8–13 wt. % and equilibrium olivines with a Fo content of 86–89 mol% [**17**]. It is common that even the most primitive olivine phenocrysts of an alkaline basalt seemingly suitable for modeling (olivine +/− clinopyroxene phenocrysts, no signs of amphibole or early pyroxene crystallization or incorporation of mafic minerals) have quite low Fo and/or Ni-content (e.g. [**34**]). In this case a proper fractionation modeling is not possible, only a rough estimation can be performed based on a comparison with similar olivine datasets containing more Fo-rich olivines. An exact limit for proper calculations cannot be specified, only suggestions for it. Based on the empirical observations of [**23**] the fractionation modeling is more reliable if the olivine crystals over the 75th percentile by Fo-content draw a steep, semi

| Sample		BRE	RAC2	SAN	SOR
GPS	N	48.403	46.032	45.811	48.226
	E	18.635	25.418	21.718	19.913
SiO_2		44,71	46,87	49,30	44,86
TiO_2		2,46	1,55	2,21	2,29
Al_2O_3		13,18	15,8	14,80	15,81
Fe_2O_3 Total		11,6	9,57	10,79	8,86
MnO		0,17	0,16	0,15	0,14
MgO		10,91	9,68	8,50	9,44
CaO		10,08	9,85	8,59	10,49
Na_2O		4,04	3,79	3,42	3,35
K_2O		1,72	1,63	1,64	2,25
P_2O_5		0,77	0,39	0,60	0,6
LOI		0	0,2	0,80	1,4
Ni		219	216	170	153
Cr		342	431	247	212

Table 1.
Composition of the basaltic samples applied for modeling. Oxides and LOI are given in wt. %, Ni and Cr in ppm. GPS: Coordinates of sample locations.

Sample	Olivine				Clinopyroxene	
	BRE	RAC2	SAN	SOR	SAN	SOR
olivine addition	**12,4**	**10,35**	**16,53**	**7,39**		
cpx addition					**5,41**	**7,56**
SiO$_2$	40,09	40,57	39,31	39,93	48,70	47,73
TiO$_2$	0,00		0,00	0,05	1,86	2,03
Al$_2$O$_3$	0,01	0,04	0,03	0,16	4,69	7,34
Fe$_2$O$_3$					3,19	3,21
FeO	11,74	11,27	16,73	15,25	4,27	3,65
MnO	0,24	0,19	0,24	0,26	0,13	0,14
MgO	46,76	47,88	43,22	44,31	14,00	13,52
CaO	0,27	0,20	0,24	0,31	22,40	22,07
Na$_2$O					0,40	0,59
NiO	0,24	0,29	0,18	0,14		0,03
Cr$_2$O$_3$	0,04	0,09	0,05	0,01	0,03	0,03

Table 2.
The amount and average composition of olivine and clinopyroxene added to the bulk rock composition (m/m %) during parental melt calculations. Olivine and pyroxene addition are based on fractionation modeling (Figure 8).
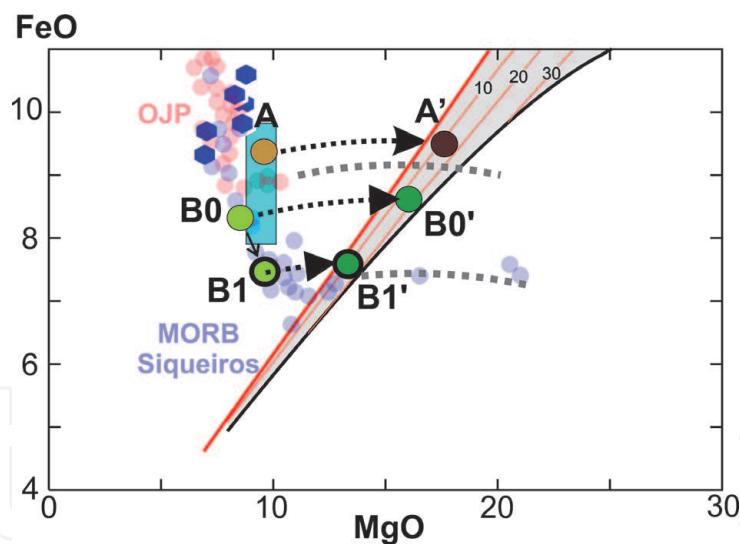
Figure 3.
Estimation of primary melts' composition - the clinopyroxene problem. Figure modified after [32]. OJP – Ontong-Java plateau basalts, MORB – Siqueiros fracture zone basalts [32], dark blue haxagons represent the compositional diversity of the monogenetic volcano of Kissomlyó (West-Hungary) [33], while the pale blue rectangle the total diversity of a volcanic field (Novohrad-Gemer/Nógrád-Gömör VF, northern Hungary and southern Slovakia) [10]. FeO and MgO are in wt. %, gray area: Primary melts' composition after accumulated fractional melting of depleted mantle peridotite. Thick red line represents the solidus, thin red lines represent the degree of melting (%). Basaltic rocks to the left of the solidus are derivatives of primary melts, while rocks to the right are richer in MgO because of accumulation of MgO-rich minerals (typically olivine). If a basaltic magma was formed only by olivine fractionation/accumulation, the primary melts composition can be estimated from the bulk rock composition using olivine addition or subtraction (gray dotted curves) [24, 32]. The pale brown circle (A) represents a basaltic rock that was formed by olivine fractionation, therefore its primary melt composition (dark brown circle, A') can be calculated by olivine addition. The pale green circle (B0) represents a basaltic rock that was formed by olivine and clinopyroxene fractionation. Its composition can be modified by adding the amount of fractionated clinopyroxene – to reach B1 (the pale green circle with a black rim). Adding olivine to the B1 melt its primary melt composition (B1, dark green circle with black rim) can be calculated. If the clinopyroxene fractionation had been ignored, the primary melts estimation by olivine addition would have been misleading (B0'). The too high MgO- and FeO-content of B0' melt would make all further estimations (e.g. temperature of the primary melt, degree of melting) inaccurate.

Calculation based on	PRIMELT2 software				Fractionation modeling presented in this article			
Sample	BRE	RAC2	SAN	SOR	BRE	RAC2	SAN	SOR
SiO_2	44,68	47,07	47,83	45,75	44,13	46,21	48,06	44,71.
TiO_2	2,17	1,46	1,78	2,21	2,15	1,39	1,77	2,1
Al_2O_3	11,57	14,88	11,86	15,22	11,53	14,17	12,63	14,01
Fe_2O_3	1,08	0,73	0,88	0,69	1,21	1,02	1,09	1,14
FeO	9,47	8,18	9,12	7,60	9,52	8,1	9,14	7,38
MnO	0,17	0,16	0,15	0,14	0,18	0,18	0,16	0,15
MgO	16,17	12,65	16,80	12,20	15,39	13,47	14,18	12,23
CaO	8,87	9,29	6,91	10,11	8,85	8,85	7,69	10,61
Na_2O	3,54	3,57	2,73	3,22	3,54	3,4	2,63	2,89
K_2O	1,51	1,53	1,31	2,16	1,51	1,46	1,53	1,91
P_2O_5	0,68	0,37	0,48	0,58	0,67	0,35	0,38	0,51
NiO	0,07	0,05	0,12	0,04	0,05	0,04	0	0,03
Cr_2O_3	0,05	0,06	0,03	0,03	0,05	0,06	0	0,03
Mg#	75,27	73,39	76,65	74,00	74,24	74,77	73,44	74,54
Olivin add. by Primelt2	14,20	7,10	23,40	6,60				

Table 3.
Primitive melt compositions calculated by the PRIMELT2 software [14] and by addition of olivine and clinopyroxene to the bulk rock based on fractionation modeling presented in this paper. Regardless of the applied method, the Mg# of the primitive melts will be quite similar in the case of olivine phyric rocks (BRE, RAC2). On the contrary, the Mg# of the primitive melts can depend on the applied method, if there were a significant amount of clinopyroxene in the sample (SAN). This means, that only by olivine addition – as the PRIMELT2 and similar softwares [14, 19, 20, 24] work – the Mg# of the primary melt will be over calculated.

vertical trend on the Fo-Ni plot and they have 89–82 mol% Fo and 2500–1200 ppm Ni content.

2. The deep-seated clinopyroxene fractionation [25] will not affect the composition of later crystallized olivines, while the presented method can reveal clinopyroxene crystallization only if it occurred together with olivine fractionation. Therefore, it cannot indicate the precipitation of clinopyroxene onto the wall rocks at great depth. To identify any modification of primary melts by reaction with mantle minerals is also beyond the limits of the presented method.

3. Since there are several variable parameters during fractionation modeling (the D_{Ni}^{ol-liq} value, the applied Fe^{3+}/Fe^{2+} ratio for the bulk rock, the amount and ratio of olivine and clinopyroxene, the composition of the intermediate melt), the calculation is a little bit cumbersome.

3. Case studies from the Carpathian-Pannonian region

3.1 Geological setting

From a volcanological and geodynamical point of view – based on its Neogene-Quaternary volcanism – the Carpathian-Pannonian Region (**Figure 4**) is a related to the broader Mediterranean area in terms of geodynamic setting [37].
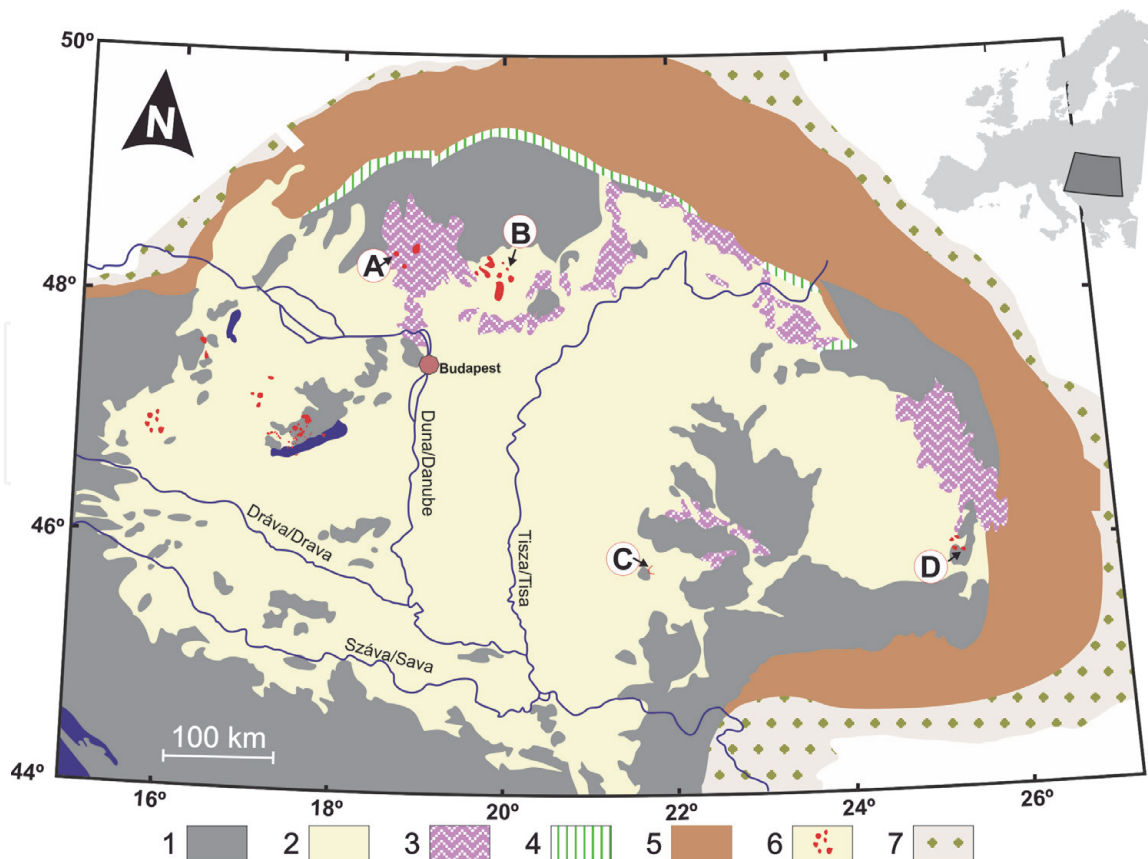
Figure 4.
Map of the Carpathian-Pannonian region after [35, 36]. 1: Pre-Cenozoic basement, 2: Neogene–Quaternary sediments, 3: Neogene calc-alkaline volcanic rocks on the surface, 4: Pieniny Klippen Belt, 5: Alp–Carpathian Flysch Belt, 6: Neogene–Quaternary alkaline basaltic volcanic fields on the surface, 7: Alp–Carpathian Molasse Belt. Sample locations. A: Putikov Vŕšok, B: Šurice (Sőreg), C: Lucaret-Sanoviţa (Lukácskő-Sziklás), D: Racoş (Alsórákos). The map insert on the upper right corner shows the position of the Carpathian-Pannonian region within Europe.

The post-Paleogene volcanic formations of the region can be divided by age and geochemical features into four groups [38]: 1) Miocene Si-rich-; 2) Miocene-Quaternary K- and high-K-; 3) Miocene-Quaternary calc-alkaline- and 4) late Miocene-Quaternary alkaline type. The latter group is represented by several alkaline basaltic monogenetic volcanic fields, some of which are deeply buried by late Miocene sediments [10, 39–41]. The most intense period of alkaline basaltic volcanism took place between 5 and 3 Ma ago. At that time numerous volcanoes formed, for example, in the Bakony-Balaton Highland Volcanic Field (e.g. [42]), in the Nógrád-Gömör/Novohrad-Gemer Volcanic Field (e.g. [40]) and in the Styrian Basin Volcanic Field (e.g. [35]). The alkaline rocks show a wide range in composition from the primitive, olivine-phyric basanites towards the more differentiated, clinopyroxene-rich phonotephrites (e.g. [10, 43, 44]). Based on their trace element content they show similarities both with the Neogene-Quaternary alkaline rocks of western and central Europe (e.g. [45, 46]) and with alkaline basaltic rocks of the Mediterranean area (e.g. [47, 48]). The driving force of the alkaline basaltic melt generation is still subject of debate as the Neogene-Quaternary basaltic volcanism of the region dominantly postdates the rifting of the Pannonian Basin and took place in the thermal inversion phase of the basin, in a compressional geodynamic regime [10, 37, 49]. There are two dominant theories for basalt generation in the area, both associate it with regional mantle flows, the differences are in the driving forces. 1) In the outer parts of the Pannonian Basin melting could have been associated with mantle upwelling related to the so-called thin-spot event, a dominantly vertical asthenospheric flow from under the deep roots of the surrounding mountain chains

or to lithospheric delamination while the sporadic volcanism in the central parts of the basin could have been related to strike-slip tectonics [10, 22, 37]. 2) The other theory comes from [50], who suggested that basaltic melt generation was caused by rather a regional, mostly horizontal mantle flow related to the north-eastward push of the Adria microplate.

3.2 Analytical methods

Whole-rock compositions were analyzed at Acme Labs (Vancouver, Canada). Major and minor elements were analyzed by ICP-ES, trace elements by ICP-MS. Petrographic descriptions were done with a Nikon YS2-T polarizing microscope using NIS-Elements Br software and an AMRAY 1830 I/T6 scanning electron microscope at the Department of Petrology and Geochemistry, Eötvös Loránd University (Budapest, Hungary). The polished and carbon-coated thin sections were analyzed with a CAMECA SX100 EMPA, equipped with one energy-dispersive and four wavelength-dispersive spectrometers at the Department of Lithospheric Research, University of Vienna (Austria). An accelerating potential of 15 kV and a beam current of 20 nA were used with at least 20 s counting time on peak position and 1 μm beam diameter. PAP correction procedure was applied on raw data. Analyses were done against natural and synthetic mineral standards: olivine (Mg), corundum (Al), quartz (Si), apatite (P), wollastonite (Ca), rutile (Ti), Mg-chromite (Cr), spessartine (Mn), almandine (Fe), Ni-oxide (Ni).

3.3 The investigated alkaline basalts

3.3.1 Samples

BRE: a massive basanitic lava rock sample (**Figures 5** and **6**) from the Putikov Vŕšok volcano, Štiavnica (Selmec) Volcanic Field. The small scoria cone and related lava flow is the youngest alkaline basaltic volcano in the Carpathian-Pannonian Region with its age of 102 ± 11 ka [51]. Sample data were taken from [22, 23].

RAC2: a trachybasaltic vesicular scoria clast (**Figures 5** and **6**) from the Racoş (Rákos) scoria cone, Perşani (Persányi) Mts. Volcanic Field. Its age is 1221 ± 11 ka [52, 53]. Sample data were taken from [22, 53].

SAN: a massive trachybasaltic lava rock sample (**Figures 5** and **6**) from the Lucaret-Sanoviţa (Lukácskő-Sziklás) volcano, Banat Volcanic Field. Its age is between 2.5–2.6 Ma [54]. Sample data were taken from [23].

SOR: a massive basanite (**Figures 5** and **6**) from a dyke cutting the maar diatreme rocks at Šurice (Sőreg), Novohrad-Gemer/Nógrád-Gömör VF. Its age is 4 ± 0.29 Ma [54]. Sample data were taken from [22].

3.3.2 Petrography

BRE: an olivine phyric massive basanite sample with porphyritic-intergranular texture (**Figure 5**). Clinopyroxene phenocrysts are very rare (olivine/clinopyroxene ratio is 19/1, total phenocryst content: 6%). Olivine phenocrysts are normal zoned, dominantly hypidiomorphic-idiomorphic with an average size of 650–700 μm, they contain idiomorphic magnetite and Cr-spinel inclusions dominantly in the crystal rims. Largest grains are often resorbed and iddingsitized along crystal rims and cleavage tracks. Hypidiomorphic-idiomorphic pale brown clinopyroxene microphenocrysts are dominantly normal-, rarely sector zoned crystals with a maximal size of 400–500 μm. They often contain idiomorphic magnetite inclusions.
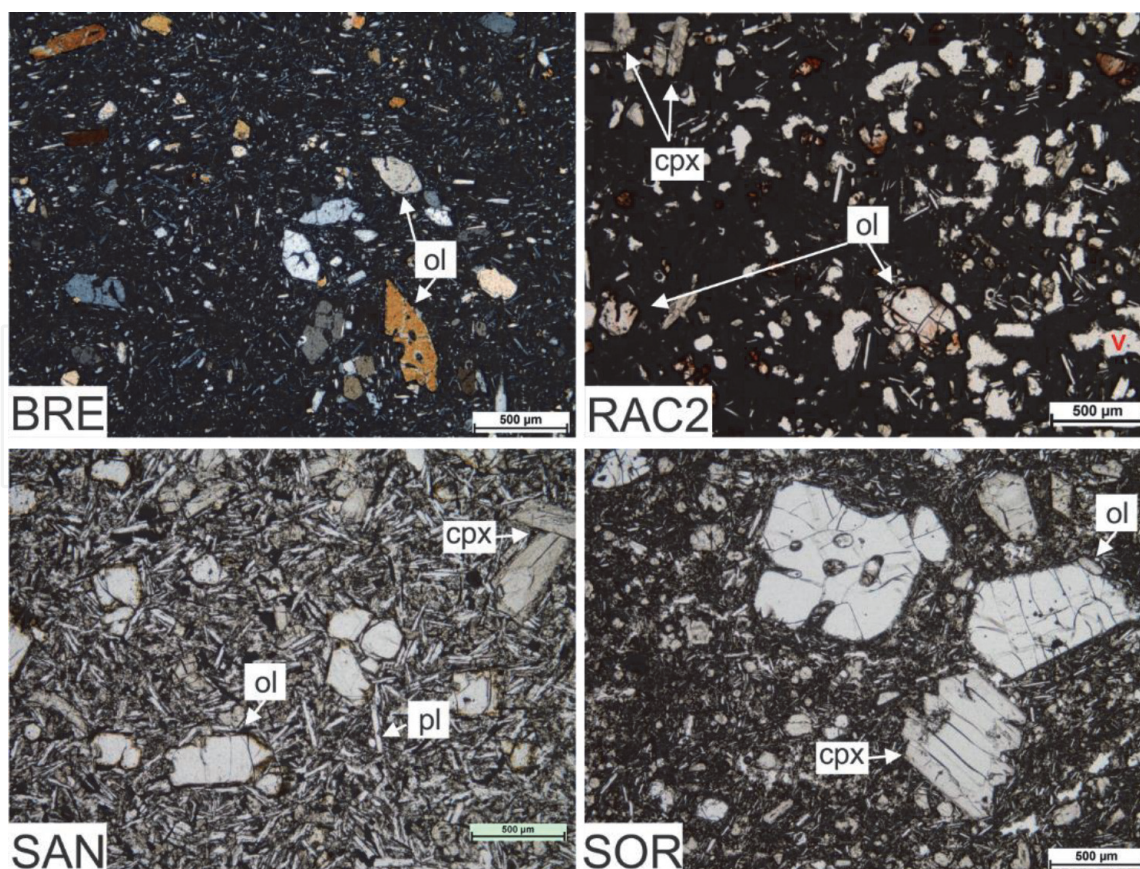
Figure 5.
Photomicrographs of the investigated samples. BRE: Olivine phyric intergranular basanite (xpl), RAC2: Olivine phyric, intersertal and moderately vesicular trachybasalt (xpl), SAN: Olivine and clinopyroxene phyric, intergranular trachybasalt (ppl), SOR: Olivine and clinopyroxene phyric, intersertal basanite (ppl). Abbreviations: Ol – Olivine, cpx – Clinopyroxene, pl. – Plagioclase, v - vesicle.
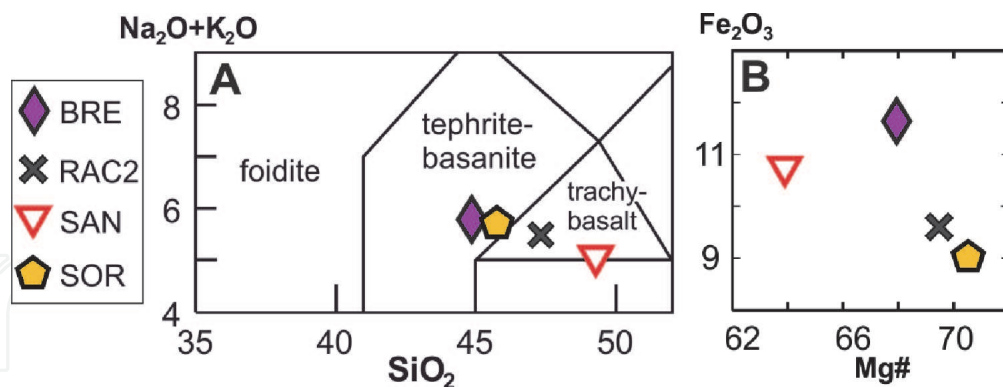

Figure 6.
A: Nomenclature of the investigated alkaline basalts (s.l.). B: They have a high or moderate Mg# (BRE: 67.9, RAC2: 69.46, SOR: 70.54, SAN: 63.9). Mg# = Mg/(Mg + Fe²⁺) × 100. By calculations of Mg# a Fe_2O_3/FeO ratio of 0.15 has been applied.

The groundmass contains plagioclase, clinopyroxene, olivine, nepheline and accessory magnetite and ilmenite.

RAC2: an olivine phyric trachybasaltic scoria clast with vesicular, porphyritic-intersertal texture (**Figure 5**). Clinopyroxene microphenocrysts are very rare (olivine/clinopyroxene ratio is 19/1, total phenocryst content: < 5%). Olivine phenocrysts are normal zoned, dominantly hypidiomorphic-idiomorphic, sometimes skeletal; with an average size of 500 μm, largest crystals reach 1250 μm. They are often strongly iddingsitized. Most oxidized grains contain few μm thick iron-oxide needles. Idiomorphic inclusions of Cr-spinel are common

in crystal rims. Hypidiomorphic-idiomorphic pale brown clinopyroxene microphe-nocrysts often form glomerocrysts. They are dominantly sector-, rarely normal zoned crystals with an average size of 300–350 μm. The groundmass contains plagioclase, clinopyroxene, olivine, glass, nepheline and accessory magnetite and ilmenite.

SAN: an olivine and clinopyroxene phyric trachybasaltic lava rock sample with porphyritic-intergranular texture (**Figure 5**). Clinopyroxene phenocrysts are quite common (olivine/clinopyroxene ratio is 4/1, total phenocryst content: 20%). Olivine phenocrysts are normal zoned, dominantly hypidiomorphic-idiomorphic, often resorbed; with an average size of 500 μm, largest crystals reach 1200 μm. They are often iddingsitized along crystal rims and cleavage tracks. Idiomorphic inclusions of Cr-spinel are common in crystal rims. Hypidiomorphic-idiomorphic pale brown clinopyroxene phenocrysts are sector zoned crystals with an average size of 300–400 μm, largest grains reach 1000 μm. They contain magnetite inclusions and they often form glomerocrysts. The groundmass contains plagioclase, clinopyroxene, olivine and accessory magnetite and ilmenite.

SOR: an olivine and clinopyroxene phyric basanitic dyke sample with slightly vesicular, porphyritic-intergranular/intersertal texture (**Figure 5**). Clinopyroxene phenocrysts are common (olivine/clinopyroxene ratio is 5/5, total phenocryst content: 8%). Olivine phenocrysts are normal zoned, dominantly hypidiomorphic-idiomorphic, often resorbed; with an average size of 650 μm, largest crystals reach 3000 μm. Idiomorphic inclusions of Cr-spinel and magnetite are common in crystal rims. Idiomorphic-hypidiomorphic pale brown clinopyroxene phenocrysts are sector-, normal- or oscillatory zoned minerals with an average size of 470 μm, largest grains reach 2000 μm. They contain magnetite inclusions. Some clinopyroxene phenocrysts have an olive-green core. Few grains of completely opacitized amphibole megacrysts can be observed. The groundmass contains plagioclase, clinopyroxene, olivine, glass, nepheline and accessory magnetite.

3.3.3 Geochemistry

Geochemical data (**Tables 1** and **2**, **Figures 6** and 7) were taken from [22, 23, 53, 55].

4. Results of olivine and clinopyroxene fractionation modeling

From two samples (BRE and RAC2) olivine crystals are fitting well to the modeled pure olivine fractionation curves that were calculated with D_{Ni}^{ol-liq} = 10. Based on this the calculated degree of olivine fractionation is 12.5 wt. % and 10.35 wt. %, respectively (**Figure 8A** and **B**). Adding this amount of olivine to the bulk rock composition the parental melt would have an Mg# of 74.24 and 74.77.

In the case of SAN and SOR only the most primitive, Mg-rich olivine crystals follow the modeled exponential olivine fractionation curve on the Fo-Ni plot and the more evolved ones draw a diagonal trend (**Figure 8C** and **D**). A D_{Ni}^{ol-liq} value of 12 and 13 were applied for SAN and SOR, respectively. The calculated degree of olivine fractionation is 9.5 wt. % for SAN and 5.5 wt. % for SOR during the initial, pure olivine crystallization period. Based on the olivine crystals that are falling onto the diagonal trend it is obvious that the evolution of both melts switched at some point from pure olivine fractionation to co-crystallization of olivine and clinopyroxene. The calculated degree of fractionation for olivine and clinopyroxene
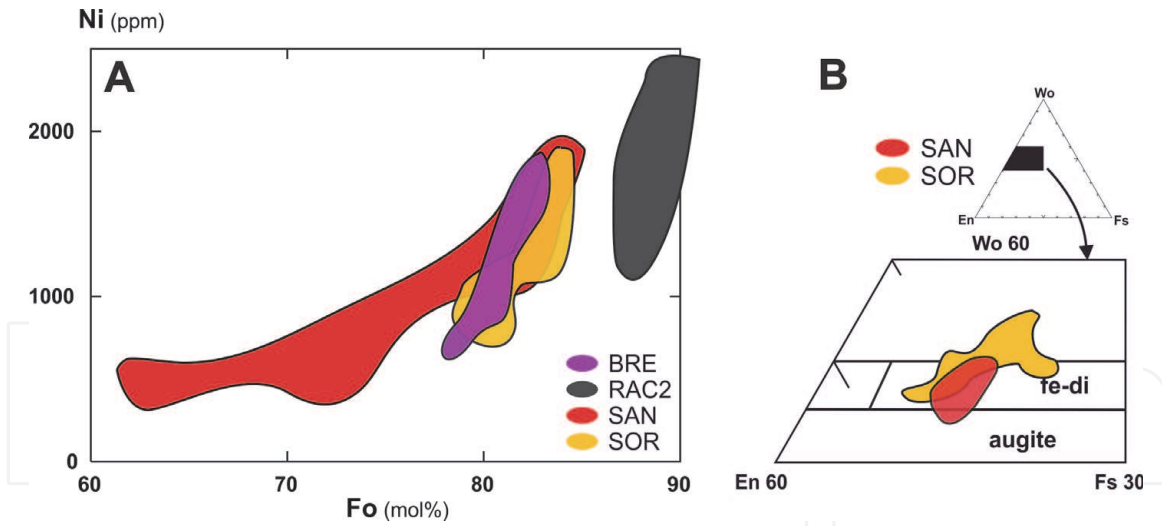
Figure 7.
A) the majority of the olivine crystals fall into the range of Fo$_{80-87}$, the cores of the normal zoned crystals are Mg rich (Fo$_{75-90}$). Their Ni-concentration correlates positively with the Fo content, Mg-rich crystal cores could reach a Ni content of 2500 ppm, while in crystal rims only 100–700 ppm of Ni can be analyzed. B) the clinopyroxene phenocrysts of the SAN trachybasalt and SOR basanite are dominantly ferroan-diopsides, rarely augites. They are dominantly sector zoned with a primitive core and a more evolved rim, MgO-content varies between 9.2 and 15.9 wt. %. CaO varies between 21.1–23.2 wt. %, higher values can be measured in crystal rims. Especially in the SOR basanite clinopyroxenes are extremely rich in Ca, several crystals exceed Wo$_{50}$.
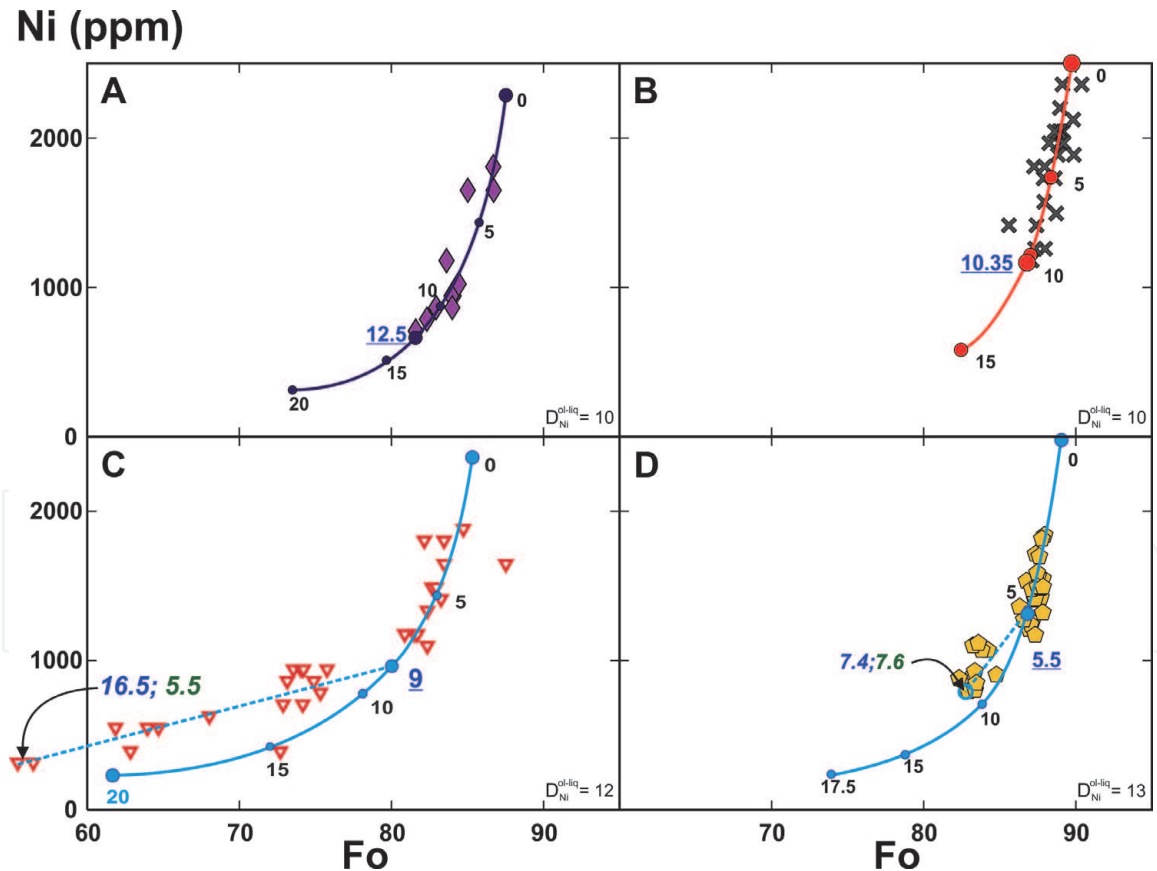

Figure 8.
Results of olivine and clinopyroxene fractionation. The composition of olivine crystals suggest only olivine fractionation in the case of the BRE basanite (A) and the RAC2 trachybasalt (B), while a significant degree of clinopyroxene fractionation played role in the formation of the SAN trachybasalt (C) and SOR basanite (D).

Calculated olivine fractionation curves are based on the indicated D_{Ni}^{ol-liq} values, black numbers indicate increasing degree of olivine fractionation along the curves. Blue, underlined numbers show the degree of pure olivine fractionation, blue and green italic numbers indicate total degree of olivine and clinopyroxene fractionation (wt. %), respectively. The most primitive olivine crystal in the RAC trachybasalt (B) is in equilibrium with the bulk rock composition and it is the starting point of the olivine fractionation curve. In the other samples the starting point is a hypothetical olivine which is in equilibrium with the bulk rock composition.

during this phase are 7 and 5.5 wt. % for SAN and 1.89 and 7.56 wt. % for SOR. The total degree of olivine and clinopyroxene fractionation is 16.5 and 5.5 wt. % for SAN and 7.39 and 7.56 wt. % for SOR. Adding this amount of the two mineral phases to the bulk rock composition the parental melt would have an Mg# of 73.44 and 74.54, respectively (**Table 3**).

5. Conclusions

The results of fractionation modeling are consistent with the petrographic observations, i.e. for the olivine phyric basalts (BRE, RAC2) only olivine fractionation have been calculated, while for those which have a considerable amount of phenocrystic clinopyroxene a significant clinopyroxene fractionation have been revealed by the model. The olivine/pyroxene ratio in the rock samples is 4/1 for SAN and 5/5 for SOR, this is fairly the same as the results of modeling (5.5/16.5 for SAN and 7.4/7.6 for SOR).

The calculated parental melts composition may resemble a mafic melt from a fertile peridotite. Parental melts composition and Mg# have been calculated with the Primelt2 software [14] too. For the olivine phyric rocks it gave a similar Mg# (BRE – 75.13, RAC2–73.27).

In the case of the SAN trachybasalt the Mg# calculated by the Primelt2 software is obviously too high (Mg# = 76.31), which is consistent with the high degree of clinopyroxene fractionation that was indicated by the fractionation modeling. This coincides with the fact that the Primelt2 program does not count on the possibility of clinopyroxene fractionation during primary melt calculations except that it gives a warning about the possible pyroxene fractionation.

The SOR basanite is little bit more interesting as the fractionation modeling have resulted the same amount of olivine and clinopyroxene fractionation, and the Mg# of the parental melts based on the modeling is somewhat higher compared to the result given by the Primelt2 [14]. In this case two important facts have to be considered. First, the modeled mineral fractionation fits very well to the petrographic observations in all case. It suggests that the pyroxene fractionation predicted by the modeling should also be realistic in the case of SOR basanite. Secondly, the Primelt2 program gives us warnings, if the calculation may be inaccurate because of pyroxenite source rocks or because of clinopyroxene fractionation. In the case of SOR basanite a pyroxene fractionation warning was given by the software, although the suggested olivine addition to reach primary melt (6.6 wt. %) is almost the same as it was given by fractionation modeling (7.39 wt. %).

The uncertainty, whether the result of the fractionation modeling or the Primelt2 is the more realistic may have arisen from two factors. Neither olivine, nor clinopyroxene is a dominant phase and probably this amount (<10 wt. %) of pyroxene is close to the limit what can be detected by the difference in primary melts' Mg#.

Despite its limitations, the presented olivine and clinopyroxene fractionation modeling based on olivine and bulk rock compositional data draw attention that it is not only olivine fractionated basalts that could be useful for primary melt calculations.

It is more important, that all possible tools have to be applied from petrographic observations to quite simple or more complicated geochemical modeling methods. We hope that the modeling presented in this chapter will inspire the reader to develop further ideas and methods to give a more realistic and better description of the fractionation process of alkaline basaltic melts.

Acknowledgements

Author details

Tamás Sági[1]*, Szabolcs Harangi[1] and Theodoros Ntaflos[2]

1 Department of Petrology and Geochemistry, Budapest, Hungary and MTA-ELTE Volcanology Research Group, Eötvös Loránd University, Budapest, Hungary

2 Department of Lithospheric Research, University of Vienna, Vienna, Austria

*Address all correspondence to: sagi.tamas@ttk.elte.hu

IntechOpen

References

[1] Németh K. Monogenetic volcanic fields: Origin, sedimentary record, and relationship with polygenetic volcanism. In: Canón-Tapia E, Szakács A, editors. What Is a Volcano? GSA; 2010. p. 43–66. DOI: 10.1130/2010.2470(04)

[2] Connor CB, Conway FM. Basaltic Volcanic Fields. In: Sigurdsson H, editor. Encyclopedia of Volcanoes. 1st ed. San Diego: Academic Press; 2000. p. 331–343. ISBN: 9780080547985

[3] Valentine GA, Perry FV. Tectonically controlled, time-predictable basaltic volcanism from a lithospheric mantle source (central Basin and Range Province, USA). EPSL. 2000; 261:201–216. DOI: 10.1016/j.epsl.2007.06.029

[4] Valentine GA, Connor BC. Basaltic Volcanic Fields. In: Sigurdsson H, editor. The Encyclopedia of Volcanoes. 2nd ed. London: Academic Press; p. 423–439. DOI: https://doi.org/10.1016/B978-0-12-385938-9.00023-7

[5] Sobolev AV, Krivolutskaya NA, Kuzmin DV. Petrology of the Parental Melts and Mantle Sources of Siberian Trap Magmatism. Petrology. 2009; 17/3:253–286. DOI: 10.1134/S0869591109030047

[6] Gazel E, Hoernle K, Carr MJ, Herzberg C, Saginor I, Bogaard VDP, Hauff F, Feigenson M, Swisher C. Plume–subduction interaction in southern Central America: Mantle upwelling and slab melting. Lithos. 2011; 121/1–4:117–134. DOI: 10.1016/j.lithos.2010.10.008

[7] Niu Y, O'Hara M. Origin of ocean island basalts: a new perspective from petrology, geochemistry, and mineral physics considerations. JGR: Solid Earth. 2003; 108:2209–2228. DOI: http://dx.doi.org/10.1029/2002JB002048

[8] Kelemen PB, Holbrook WS. Origin of thick, high-velocity igneous crust along the U.S. East Coast Margin. JGR: Atmospheres. 1995; 100/B7:10077–10094. DOI: 10.1029/95JB00924

[9] Wang K, Plank T, Walker JD, Smith EI. A mantle melting profile across the Basin and Range, SW USA. JGR: Solid Earth. 2002; 107/B1:ECV 5–1–ECV 5–21. DOI: 10.1029/2001JB000209

[10] Harangi Sz, Jankovics MÉ, Sági T, Kiss B, Lukács R, Soós I. Origin and geodynamic relationships of the late Miocene to quaternary alkaline basalt volcanism in the Pannonian basin, eastern-central Europe. IJES. 2015; 104:2007–2032. DOI: https://doi.org/10.1007/s00531-014-1105-7

[11] Fitton JG, James D, Leeman WP. Basic magmatism associated with late Cenozoic extension in the western United States: compositional variations in space and time. JGR: Atmospheres. 1991; 96:13693–13711. DOI: 10.1029/91JB00372

[12] Pilet S, Baker MB, Stolper M. Metasomatized Lithosphere and the Origin of Alkaline Lavas. Science. 2008; 320 (5878):916–919. DOI: https://doi.org/10.1126/science.1156563

[13] Mayer B, Jung S, Romer R, Pfänder JA, Klügel A, Pack A, Gröner E. Amphibole in alkaline basalts from intraplate settings: implications for the petrogenesis of alkaline lavas from the metasomatised lithospheric mantle. Contrib Mineral Petrol. 2014; 167:989. DOI: 10.1007/s00410-014-0989-3

[14] Herzberg C, Asimow PD. Petrology of some oceanic island basalts: PRIMELT2.XLS software for primary magma calculation. G3. 2008; Q09001. DOI: http://doi.org/10.1029/2008GC002057

[15] Niu Y. The origin of alkaline lavas. Science. 2008; 320:883–884. DOI: 0.1126/science.1158378

[16] Pilet S, Ulmer P, Villiger S. Liquid line of descent of a basanitic liquid at 1.5 Gpa: constraintson the formation of metasomatic veins. Contrib Mineral Petrol. 2009; 159:621–643. DOI: 10.1007/s00410-009-0445-y

[17] Herzberg C. Identification of source lithology in the Hawaiian and Canary Islands: implications for origins. Journal of Petrology. 2011; 52:113–146. DOI: https://doi.org/10.1093/petrology/egq075

[18] Smith IEM, Blake S, Wilson CJN, Houghton BF. Deep-seated fractionation during the rise of a small-volume basalt magma batch: Crater Hill, Auckland, New Zealand. Contrib Mineral Petrol. 2008; 155/4:511–527. DOI: https://doi.org/10.1007/s00410-007-0255-z

[19] Lee C-TA, Luffi P, Plank T, Dalton H, Leeman WP. Constraints on the depths and temperatures of basaltic magma generation on Earth and other terrestrial planets. EPSL. 2009; 279:20–33. DOI: https://doi.org/10.1016/ j.epsl.2008.12.020

[20] Kimura J-I, Kawabata H. Ocean Basalt Simulator version 1 (OBS1): Trace element mass balance in adiabatic melting of apyroxenite-bearing peridotite. — G3. 2015; 16:267–300. DOI: http://doi.org/10.1002/2014GC005606

[21] Putirka KD, Perfit M, Ryerson FJ, Jackson MG. Ambient and excess mantle temperatures, olivine thermometry, andactive vs. passive upwelling. Chemical Geology. 2007; 241/3–4:177–206. DOI: https://doi.org/10.1016/j.chemgeo.2007.01.014

[22] Sági T. A Persányi-hegység, a Selmeci- és a Nógrád-Gömöri vulkáni terület alkáli bazaltjainak petrogenezise (Petrogenesis of the alkaline basalts of the Perşani Mts., Štiavnica and Novohrad-Gemer Volcanic Fields) [PhD thesis]. Budapest, Eötvös Loránd University; 2018. DOI: 10.15476/ELTE.2018.125

[23] Sági T, Jankovics MÉ, Kiss B, Ntaflos T, Harangi Sz. Új módszer alkáli bazaltos magmák olivin- és klinopiroxén-frakcionációjánakmodellezésére (A new method for the olivine- and clinopyroxene fractionation modelling of alkaline basaltic magmas). Földtani Közlöny. 2018; 148/3:273–292. DOI: 10.23928/foldt.kozl.2018.148.3.273

[24] Herzberg C, Asimow PD. PRIMELT3 MEGA.XLSM software for primary magma calculation: peridotite primary magma MgO contents from the liquidus to the solidus. G3. 2015; 16:563–578. DOI: 10.1002/2014GC005631

[25] Putirka KD. Mantle potential temperatures at Hawaii, Iceland, and the mid-ocean ridge system, as inferred from olivine phenocrysts: Evidence for thermally driven mantle plumes. G3. 2005; 6:Q05L08. DOI: 10.1029/2005GC000915

[26] Sato H. Nickel Content of Basaltic Magmas - Identification of Primary Magmas and a Measure of Degree of Olivine Fractionation. Lithos. 1977; 10/2:113–120. DOI: https://doi.org/10.1016/0024-4937(77)90037-8

[27] Kawabata H, Hanyu T, Chang Q, Kimura JI, Nichols ARL, Tatsumi Y. The Petrology and Geochemistry of St. Helena Alkali Basalts: Evaluation of the Oceanic Crust-recycling Model for HIMU OIB. Journal of Petrology. 2011; 52/4:791–838. DOI: https://doi.org/10.1093/petrology/egr003

[28] Villemant B, Jaffrezic H, Joron JL, Treuil M. Distribution Coefficients of Major and Trace-Elements – Fractional Crystallization in the Alkali Basalt Series of Chaine-Des-Puys (Massif Central, France). Geochimica et Cosmochimica Acta. 1981; 45/11:1997–2016. DOI: https://doi.org/10.1016/0016-7037(81)90055-7

[29] Hart SR, Davis KE. Nickel Partitioning between Olivine and Silicate Melt. EPSL. 1978; 40/2:203–219. DOI: https://doi.org/10.1016/0012-821X (78)90091-2

[30] Lemarchand F, Villemant B, Calas G. Trace-Element Distribution Coefficients in Alkaline Series. Geochimica et Cosmochimica Acta. 1987; 51/5:1071–1081. DOI: https://doi.org/10.1016/0016-7037(87)90201-8

[31] Laubier M, Grove TL, Langmuir CH. Trace element mineral/melt partitioning for basaltic and basaltic andesitic melts: An experimental and laser ICP-MS study with application to the oxidation state of mantle source regions. EPSL. 2014; 392: 265–278. DOI: https://doi.org/10.1016/j.epsl.2014.01.053

[32] Herzberg C, Asimow PD, Arndt, NT, Niu Y, Lesher CM, Fitton JG, Cheadle MJ, Saunders AD. Temperatures in ambient mantle and plumes: constraints from basalts, picrites and komatiites. G3. 2007; 8: Q02006. DOI: http://doi.org/10.1029/2006GC001390

[33] Jankovics MÉ, Harangi Sz, Németh K, Kiss B, Ntaflos T. A complex magmatic system beneath the Kissomlyó monogenetic volcano (western Pannonian Basin): evidence from mineral textures, zoning and chemistry. JVGR. 2015; 301:38–55. DOI: https:// doi.org/10.1016/j.jvolgeore s.2015.04.010

[34] Embey-Isztin A, Dobosi G. Composition of olivines in the young alkali basalts and their peridotite xenoliths from the Pannonian Basin. Annales Musei Historico-naturalis Hungarici. 2007; 99:5–22. ISSN: 0521–4726

[35] Ali S, Ntaflos T, Upton BGJ. Petrogenesis and mantle source characteristics of Quaternary alkaline mafic lavas in the western Carpathian–Pannonian Region, Styria, Austria. Chemical Geology. 2013; 337–338:99–113. DOI: http://doi.org/10.1016/ j. chemgeo.2012.12.001

[36] Kováč M, Márton E, Oszczypko N, Vojtko R, Hók J, Králipková S, Plašienka, D, Klučiar T., Hudáčková N, Oszczypko-Clowes M. Neogene palaeogeography and basin evolution of the Western Carpathians, Northern Pannonian domain and adjoining areas. Global and Planetary Change. 2017; 155: 133–154. DOI: https://doi.org/10.1016/j.gloplacha.2017.07.004

[37] Harangi Sz, Lenkey L. Genesis of the Neogene to Quaternary volcanism in the Carpathian–Pannonian region: Role of subduction, extension, and mantle plume. In: Beccaluva L, Bianchini G, Wilson M. editors. Cenozoic Volcanism in the Mediterranean Area. Boulder: GSA; 2007. p. 67–92. ISBN: 9780813724188

[38] Harangi Sz. Neogene to Quaternary volcanism of the Carpathian–Pannonian Region — a review. Acta Geologica Hungarica. 2001; 44/2–3:223–258. ISSN: 02365278

[39] Balázs E, Nusszer A. Magyarország medenceterületeinek kunsági (pannóniai s. str.) emeletbeli vulkanizmusa. (Lower Pannonian Volcanism of the basin areas of Hungary). A Magyar Állami Földtani Intézet Évkönyve (Yearbook of the Hungarian Geological Institute). 1987; 69:95–113.

[40] Konečný V, Balogh K; Orlický O, Vass D, Lexa J. Timing of the Neogene-Quaternary Alkaline Basalt Volcanism in Central and Southern Slovakia (Western Carpathians). Geologica Carpathica Special Issue (Proceedings of XVII. Congress of Carpathian-Balkan Geological Association, Bratislava, September 1–4, 2002). 2002; 50/3.

[41] Seghedi I, Popa RG, Panaiotu CG, Szakács A, Pécskay Z. Short-lived eruptive episodes during the construction of a Na-alkalic basaltic field (Perşani Mountains, SE Transylvania, Romania). Bull Volcanol. 2016; 78:69. DOI: https://doi.org/10.1007/s00445-016-1063-y

[42] Martin U, Németh K. Mio/Pliocene Phreatomagmatic Volcanism in the Western Pannonian Basin. Geologica Hungarica, series Geologica. 2004; 26:1–192 p.

[43] Embey-Isztin A, Downes H, James DE, Upton BGJ, Dobosi G, Ingram GA, Harmon RS, Scharbert HG. The Petrogenesis of Pliocene Alkaline Volcanic-Rocks from the Pannonian Basin, Eastern Central-Europe. Journal of Petrology. 1993; 34/2:317–343. DOI: https://doi.org/10.1093/petrology/34.2.317

[44] Dobosi G, Downes H, Mattey D, Embey-Iszti A. Oxygen isotope ratios of phenocrysts from alkali basalts of the Pannonian Basin: evidence for an O-isotopically homogeneous upper mantle beneath a subduction-influenced area. Lithos. 1998; 42:213–223. DOI: https://doi.org/10.1016/S0024-4937(97)00043-1

[45] Embey-Isztin A, Dobosi G. Mantle source characteristics for Miocene–Pleistocene alkali basalts, Carpathian–Pannonian Region: a review of trace elements and isotopic composition. Acta Vulcanologica. 1995; 7/2:155–166.

[46] Lustrino M, Wislon M. The circum-Mediterraneum anorogenic Cenozoic igneous province. Earth Science Reviews. 2007; 81:1–65. DOI: 10.1016/j.earscirev.2006.09.002

[47] Harangi Sz, Downes H, Seghedi I. Tertiary-Quaternary subduction processes and related magmatism in the Alpine-Mediterranean region. In: Gee DG, Stephenson RA, editors. European Lithosphere Dynamics. London: Mem Geol Soc Lond; 2006.

p. 167–190. DOI: 10.1144/GSL.MEM.2006.032.01.10

[48] Beccaluva L, Bianchini G, Natali C, Siena F. Geodynamic control on orogenic and anorogenic magmatic phases in Sardinia and Southern Spain: inferences for the Cenozoic evolution of the western Mediterranean. Lithos. 2011; 123:218–224. DOI: 10.1016/j.lithos.2011.01.007

[49] Horváth F, Musitz B, Balázs A, Végh A, Uhrin A, Nádor A, Koroknai B, Pap N, Tóth T, Wórum G. Evolution of the Pannonian basin and its geothermal resources. Geothermics. 2015; 53:328–352. DOI: 10.1016/j.geothermics.2014.07.009

[50] Kovács I, Falus Gy, Suart G, Hidas K, Szabó Cs, Flower MFJ, Hegedűs E, Posgay K, Zilahi-Sebess L. Seismic anisotropy and deformation patterns in upper mantle xenoliths from the central Carpathian–Pannonian region: Asthenospheric flow as a driving force for Cenozoic extension and extrusion? Tectonophysics. 2012; 514:168–179. DOI: https://doi.org/10.1016/j.tecto.2011.10.022

[51] Šimon L, Maglay J. Dating of sediments underlying the Putikov vŕšok volcano lava flow by the OSL method. Mineralia Slovaca. 2005; 37:7–40.

[52] Panaiotu CG, Jicha BR, Singer BS, Tugui A, Seghedi I, Panaiotu AG, Necula C. 40Ar/39Ar chronology and paleomagnetism of Quaternary basaltic lavas from the Perşani Mountains (East Carpathians). Physics of the Earth and Planetary Interiors. 2013; 221:1–24. DOI: 10.1016/j.pepi.2013.06.007

[53] Harangi Sz, Sági T, Seghedi I, Ntaflos T. A combined whole-rock and mineral-scale investigation to reveal the origin of the basaltic magmas of the Perşani monogenetic volcanic field, Romania, eastern–central Europe.

Lithos. 2013; 180–181:43–57. DOI:
https://doi.org/10.1016/j.lith
os.2013.08.025

[54] Balogh K. A K/Ar és 40Ar/39Ar
geokronológia fejlesztése és
alkalmazása, I. rész (Development and
geochronological application of the K/
Ar and 40Ar/39Ar method, part I.)
[DsC thesis]. Debrecen: Hungarian
Academy of Sciences, 2006. 229 p.

[55] Tschegg C, Ntaflos T, Kiraly F,
Harangi Sz. High temperature corrosion
of olivine phenocrysts in Pliocene
basalts from Banat, Romania. Austrian
Journal of Earth Sciences. 2013; 103:
101–110.